

Mean-flow characteristics of High Reynolds Number Turbulent Boundary Layers from Two Facilities

By Jens M. Österlund¹, Arne V. Johansson¹,
Hassan M. Nagib² & Michael H. Hites²

¹Dept. of Mechanics, KTH, SE-100 44 Stockholm, Sweden

²Illinois Institute of Technology, Chicago, IL 60616, USA

To be submitted

The mean flow characteristics of a zero-pressure-gradient turbulent boundary layer were investigated through extensive measurements in two different high-quality flow facilities, the MTL wind-tunnel at KTH and the NDF wind-tunnel at IIT. The study was focused on exploring the characteristics of the overlap region. The wall shear stress is a key quantity in this type of study and was in both the present experiments determined through oil-film interferometry. Also a large range of Reynolds numbers is crucial for this type of study. We here report results, for Reynolds numbers based on the momentum thickness ranging from 2,500 to 27,000. Contrary to the conclusions of some recent publications, the present analysis of the data reveals no significant Reynolds number dependence for the parameters describing the overlap region using the classical logarithmic relation. However, the data analysis demonstrates that the viscous influence extends within the buffer region to $y^+ \approx 200$, compared to the previously assumed limit of $y^+ \approx 50$. Therefore, the lowest Re_θ value where a significant logarithmic overlap region exists is about 6,000. This probably explains the Reynolds number dependence had been found from the data analysis of some previous experiments. The parameters of the logarithmic overlap region are here found to be constant and are estimated to be: $\kappa = 0.38$, $B = 4.1$ and $B_1 = 3.6$.

1. Introduction

In the traditional theory, the overall character of a turbulent boundary layer is given by the two disparate inner and outer length scales. The outer length scale is commonly taken as the thickness of the boundary layer δ , and the inner length scale as the viscous length $l^* = \nu/u_\tau$, where $u_\tau = \sqrt{\tau_w/\rho}$ is the friction velocity, τ_w is the skin friction and ρ is the density of the air. Dimensional analysis of the dynamic equations with boundary conditions leads to a scaling

of the mean velocity profile in the inner and the outer parts of the boundary layer in the form:

$$\overline{U}^+ = \frac{\overline{U}}{u_\tau} = f(y^+); \quad \overline{y}^+ = \frac{yu_\tau}{\nu} \quad (1)$$

$$\frac{U_\infty - \overline{U}}{u_\tau} = F(\eta); \quad \eta = \frac{y}{\delta} \quad (2)$$

At sufficiently large Reynolds numbers, it is assumed that there is a region of overlap, $\nu/u_\tau \ll y \ll \delta$, where the law of the wall (1) and the defect law (2) simultaneously hold. Matching (Millikan 1938) the relations (1) and (2) gives one of the classical results in turbulence theory, *i.e.*, the logarithmic overlap region: in inner variables,

$$\overline{U}^+ = \frac{1}{\kappa} \ln(y^+) + B \quad (3)$$

and in outer variables

$$\frac{U_\infty - \overline{U}}{u_\tau} = -\frac{1}{\kappa} \ln(\eta) + B_1. \quad (4)$$

By combining Equations (3) and (4) one obtains the logarithmic skin friction law

$$\frac{U_\infty}{u_\tau} = \frac{1}{\kappa} \ln\left(\frac{\delta u_\tau}{\nu}\right) + B + B_1. \quad (5)$$

Recently, due primarily to inconsistencies with trends of experimental data, several researchers have investigated alternatives to the classical theory Zagarola & Smits (1998*b,a*); George *et al.* (1996); Barenblatt & Chorin (1999).

Based on extensive data from two independent experiments, this investigation targets three main issues related to the overlap region between the inner and outer parts of turbulent boundary layers under zero pressure gradient, *viz.*, the functional form of the overlap, the extent of the overlap and any Reynolds number dependence that may exist in the overlap parameters.

2. Experimental Setup

The experiments were carried out in the MTL-wind tunnel (Johansson 1992) at the department of mechanics, KTH and the NDF-tunnel at IIT (Nagib *et al.* 1994; Hites 1997).

At KTH a seven meter long flat plate was mounted in the test section of the MTL wind-tunnel. Zero pressure gradient was achieved by adjusting the walls opposite to the plate. The variation of the velocity outside the boundary layer was measured to be less than 0.2% of the free stream velocity. The boundary layer was tripped using DYMO brand embossing tape with letters "V". Measurements of the turbulent boundary layer were performed at five different streamwise stations, $x = 1.5, 2.5, 3.5, 4.5,$ and 5.5 m at 10 different

wind-tunnel speeds. Hot-wire anemometry probes, mounted on a traversing system protruding from the plate, were used to measure the velocity in the boundary layer. Before the wind tunnel was turned on, the initial distance from the wall to the probe was measured, with an accuracy of $\pm 5\mu\text{m}$, using a microscope. During the traversing process, a distance measuring laser system was mounted under the plate looking directly at the wire through a Plexiglas plug. This arrangement made it possible to continuously measure the sensor distance to the wall, for $y < 2$ mm, when the tunnel was running. The error of the absolute wall distance measurements was $\pm 5\mu\text{m}$.

At IIT a 9 m long cylinder was mounted in the test section of the NDF-tunnel. Measurements were taken (Hites 1997; Ornt 1999) along the boundary layer of this axisymmetric body (0.46 m diameter), at $x = 1.84, 3.65, 7.33$ m, using five different free-stream velocities. A short fetch of sandpaper roughness was used to trigger the transition in the boundary layer at the same location for all velocities. The traversing mechanism was mounted in the side wall of the NDF wind tunnel and the initial position of the probe with respect to the surface was regularly monitored using an optical cathetometer from outside the test section. The adjustable test-section ceiling was also positioned for a zero-pressure gradient along the cylinder model. The high quality of the test section flow has been previously reported by Nagib *et al.* (1994). Additional details are found in the PhD thesis of Hites (1997).

3. Skin Friction Measurements

3.1. Near-wall method

One method to determine the skin friction is to measure the mean velocity gradient close to the wall in the viscous sub-layer; i.e., in the region where $y^+ < 3$. This method is not practical when making measurements at high Reynolds numbers and/or low Prandtl numbers. In the current experiments this would require performing accurate measurements closer than $30\mu\text{m}$ from the wall, which is not possible with hot-wire techniques. Therefore, a new method to determine the wall-shear stress has been developed. The method is based on determining the skin friction from the measured velocity profile in the inner layer, using the law of the wall (Equation (1)) at a distance from the wall where it is possible to make accurate measurements. The measured velocity profile is fitted to the law-of-the-wall in a procedure minimizing the mean-square error. This is similar to what is done when using the Clauser method in the logarithmic region of the velocity profile. The problem with using the Clauser method is obvious since it assumes similarity in the overlap region, which is precisely what we want to investigate. For similar reasons the use of Preston tubes is not desirable here.

In order to utilize accurate mean velocity measurements to evaluate the wall-shear stress, the form of the law-of-the-wall was chosen from available

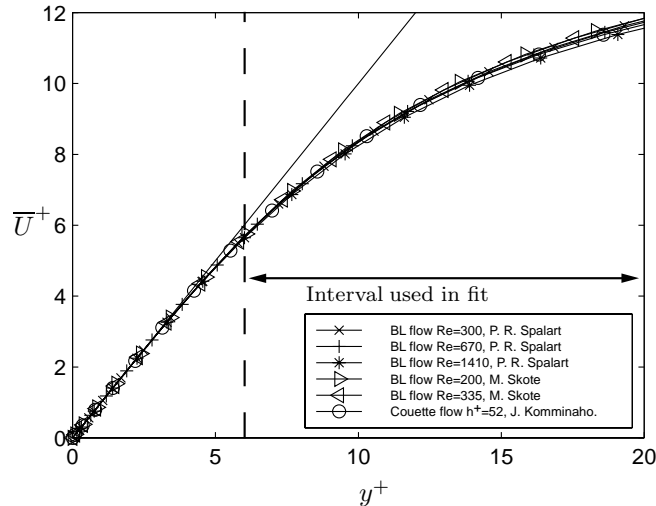


FIGURE 1. Mean velocity from DNS of boundary layer by Spalart (1988) and Skote *et al.* (1998), and Couette flow by Komminaho *et al.* (1996).

direct numerical simulations (DNS) of turbulent shear flows. Since the DNS data are available with great detail in the region where accurate measurements can be achieved and where the measurements are still well within the inner layer, the range $6 < y^+ < 20$ was selected for this near-wall method. In Figure 1, the mean velocity profiles from several recent direct numerical simulations are reproduced. The Couette flow simulation was chosen since it most closely resembles the flow in the inner part of a high Reynolds number turbulent boundary layer. In particular, there is no streamwise pressure gradient in this flow and the total shear stress is constant, over a range of distances from the wall, as shown in Figure 2. Note that for this flow $\bar{\tau}^+ = 1$ for all y^+ .

3.2. Oil-film interferometry

Oil film interferometry was used in both experiments to measure the skin friction. The basic principle of the method is to measure the deformation of a thin film of oil when subjected to a shear stress on its top surface. A simple and convenient measurement technique is based on illuminating the oil-film by a monochromatic light and recording the change in the generated interference pattern, e.g., with a video camera (see Figure 3). The skin friction is determined from the recording of the fringe patterns and utilizing the wave length of the light source λ , the kinematic viscosity of the oil ν , the refractive index of the oil n , and the angle of the camera axes to the normal of the plate α . The accuracy of the mean skin friction value $\bar{\tau}_w$ measured by this oil-film method is better than $\pm 4\%$ (Fernholz *et al.* 1996).

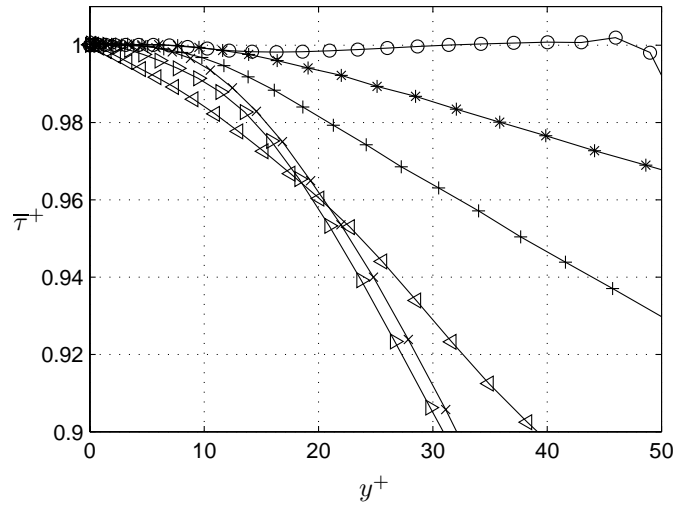


FIGURE 2. Total shear stress from DNS calculations; for legend see Figure 1

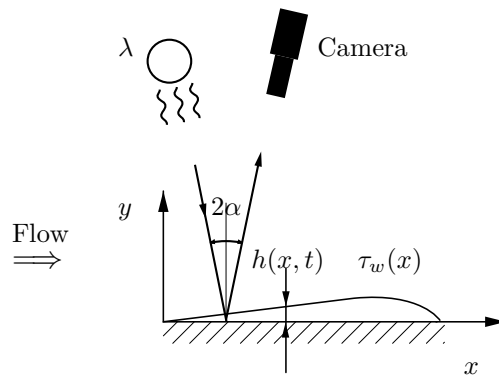


FIGURE 3. Schematic of oil-film technique.

4. Skin Friction Results

The results from the skin friction measurements are summarized in Figure 1. The oil-film measurements from the KTH experiments are plotted together with the skin friction law derived from the similar IIT experiments. Based on the velocity profiles from the KTH experiments the skin friction was also evaluated using the near-wall method.

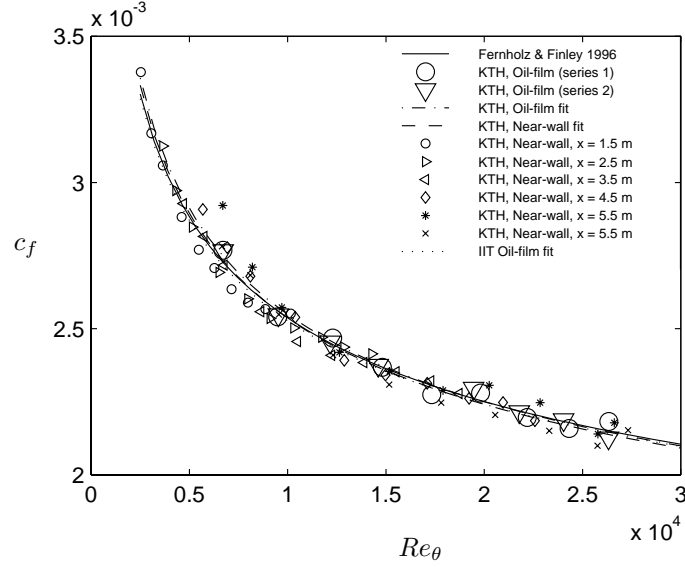


FIGURE 4. Skin-friction coefficient using the oil-film and near-wall methods (paper 8), shown with best-fit logarithmic friction laws from Equation (6) and Fernholz & Finley (1996).

A fit to c_f by a variant of the logarithmic skin friction law (Equation (5)), namely

$$c_f = 2 \left[\frac{1}{\kappa} \ln(Re_\theta) + C \right]^{-2}, \quad (6)$$

was made for each of the data sets and the friction velocity used in scaling the data was then calculated as $u_\tau = U_\infty (c_f/2)^{1/2}$. The value of the von Kármán constant determined in this way was $\kappa = 0.384$ and the additive constant was found to be $C = 4.08$. However, it is not possible to determine the additive constants B and B_1 by this method.

In Figure 1, the results from the oil-film measurements together with the values of the skin friction determined from the mean velocity by the near-wall technique (paper 8), are shown together with the calculated best fits using Equation (6). The resulting logarithmic skin-friction laws agree very well with each other and also with the correlation by Fernholz & Finley (1996).

5. Mean Velocity

In Figure 5, the mean velocity profiles from the 70 experiments at KTH and the 15 data sets from the IIT experiments are shown in inner scaling. A very nice collapse of the data is displayed even far out from the wall. A logarithmic profile with constants from a best fit to the KTH data is also shown. The

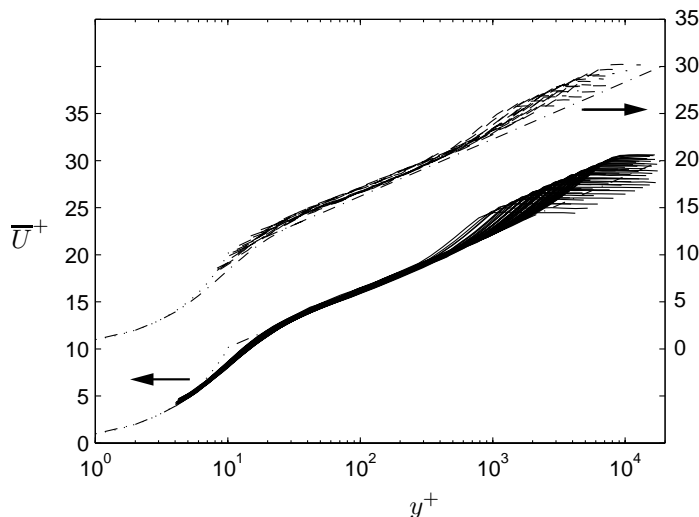


FIGURE 5. Mean velocity inner scaling; solid lines: data from KTH, dashed lines: data from IIT, dash-dotted lines: log-law with constants $\kappa = 0.38$ and $B = 4.1$, and note shift of axis.

constants were found to be: $\kappa = 0.38$, $B = 4.1$ and $B_1 = 3.6$, see section 6. The IIT experiment gives the same value of the von Kármán constant, κ , but different values of the additive constants, which is seen as a vertical shift, from the KTH log-profile, in figures 5 and 6.

In Figure 6 the same data are replotted using classical outer scaling and the collapse is very good, although the IIT data again shows another value of the additive constant.

The boundary layer thickness δ is a quantity which cannot be exactly defined and is commonly taken as y when $\bar{U}/U_\infty = 0.95$ here denoted δ_{95} and used throughout this article. Other definitions that are often used include the Rotta-Clauser length $\Delta = \delta^* U_\infty / u_\tau$, first used by Rotta (1950), or the Coles δ_{ct} which is defined as the distance to the wall of the point of maximum deviation from the log law, in the outer part of the boundary layer. Comparisons between the defect mean-velocity profiles in the outer part of the boundary layer using different outer length scales are shown in Figure 7. To put them all on the same axis each scaling is multiplied by the mean of the ratio between the length scale under consideration and δ_{95} , for all Reynolds numbers.

Except for the scaling with θ , which is somewhat worse than the others, no clear preference for an outer scale can be derived from this figure. However, the Rotta-Clauser length scale, Δ , has the advantage of being an integral length

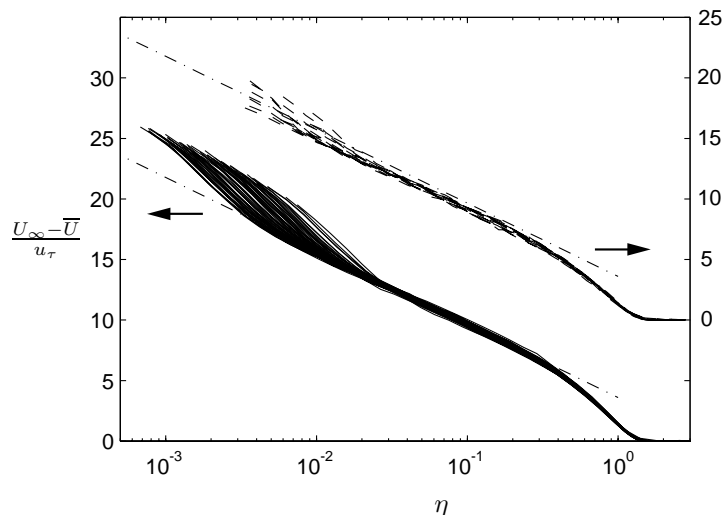


FIGURE 6. Mean velocity outer scaling; solid lines: data from KTH, dashed lines: data from IIT, dash-dotted lines: log-law with constants $\kappa = 0.38$ and $B_1 = 3.6$, and note shift of axis.

scale and is thus easier to determine from experimental data, also with relatively few data points across the boundary layer.

To further investigate the mutual scaling between the thicknesses we show the normalized outer length scale ratios in Figure 8. The ratios are multiplied by the average ratio over all Reynolds numbers to better show the variation. The Rotta-Clauser and Coles boundary layer thicknesses again show a similar behavior and increase slightly with Re_θ . The ratio of the momentum thickness and δ_{95} exhibits the opposite behavior and decreases with Re_θ . This explains the poor scaling with θ in Figure 7.

Coles (1962) formed a uniformly valid velocity profile by adding the inner (1) and outer (2) solutions and removing the common part to arrive at:

$$\begin{aligned} \bar{U}^+ &= f(y^+) - F(y/\delta_{ct}) + F(y/\delta_{ct})_{cp} \\ &= f(y^+) + \frac{\Pi}{\kappa} w(y/\delta_{ct}), \end{aligned} \quad (7)$$

where $w(y/\delta_{ct})$ is the Coles wake function and Π the wake strength. The wake function is normalized so that $w(1) = 2$. In Figure 9, the calculated wake strength, Π , is shown as a function of Re_θ . For low values of Re_θ , the magnitude of Π is increasing with increasing Re_θ , but for $Re_\theta > 10,000$ the data indicate an approximately constant value. A slightly decreasing trend was observed by Coles for intermediate Reynolds numbers. Here, any such trend is

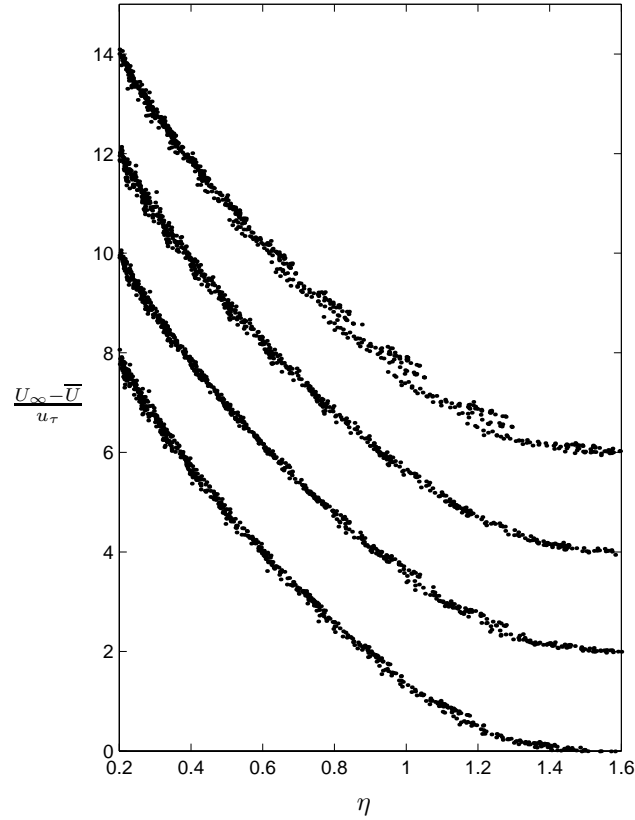


FIGURE 7. Mean velocity in outer scaling with the different definitions for η : y/δ_{95} , $(y/\Delta)\langle\Delta/\delta_{95}\rangle$, $(y/\delta_{ct})\langle\delta_{ct}/\delta_{95}\rangle$ and $(y/\theta)\langle\theta/\delta_{95}\rangle$, where averages over Re_θ are denoted by $\langle\dots\rangle$; note data is shifted upwards with an increment of 2 units between each set.

hardly visible. A difference from the data analysis of Coles is that we here have used the new values ($\kappa = 0.38$, $B = 4.1$) for the log-layer parameters. This explains the lower value of Π obtained here as compared to the value of about 0.55 found by Coles (with $\kappa = 0.41$, $B = 5$).

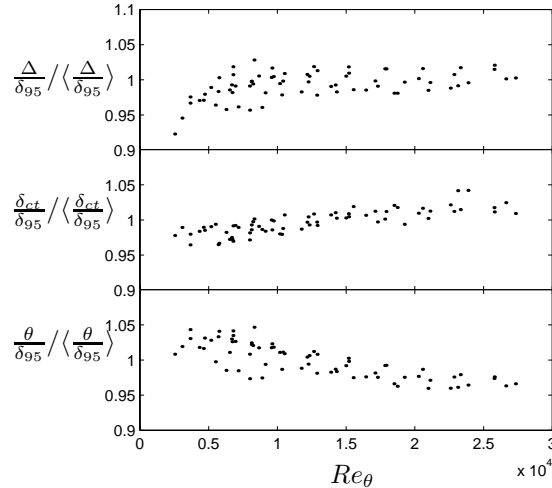


FIGURE 8. Normalized outer length scale ratios, where $\langle \dots \rangle$ denotes mean values for all Re_θ cases.

6. Scaling in the overlap region

In order to investigate the scaling in the overlap region, a normalized slope of the mean velocity profile,

$$\Xi = \left(y^+ \frac{d\bar{U}^+}{dy^+} \right)^{-1}, \quad (8)$$

was utilized. In a logarithmic region of the profiles Ξ is constant and equal to κ . The value of Ξ was calculated by taking an average of the individual profiles at a constant wall distance in inner scaling while omitting the part of the profiles where $\eta > M_o$. Similarly, the profiles were again averaged at constant outer-scaled distances from the wall for $y^+ > M_i$. The parameters M_i and M_o are the inner and outer limits of the overlap region. In Figures 10 and 11, the averaged Ξ is shown together with error bars representing a 95% confidence interval. A region where a nearly constant Ξ very accurately represents the data is evident in both figures. This clearly supports the existence of a logarithmic overlap region within the appropriate range of the parameters M_i and M_o . The choice of the appropriate limits was subsequently selected based on the y values where the error bar deviates significantly from the horizontal line in the figures. This was based on an iteration of the limits until a consistent result was obtained. The resulting values for the inner and outer limits are $M_i \approx 200$ and $M_o \approx 0.15$, respectively. Taking κ as the average value within the determined limits gives a κ of about 0.38.

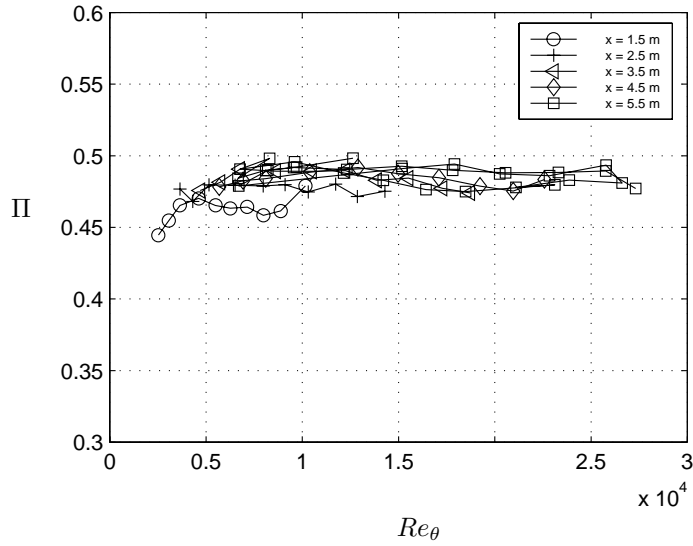


FIGURE 9. Strength of the wake component, Π . Measurements from five different X-positions is shown. Note that this is not directly comparable to Coles strength of the wake since the new set of log-law constants was used, see section 6.

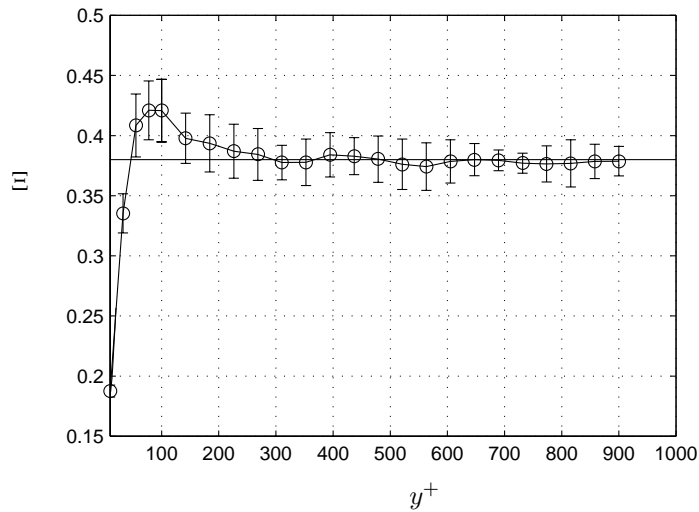


FIGURE 10. Normalized slope of mean profile, Ξ , shown in inner scaling; only the part of the profiles in which $\eta < 0.15$ was used and the horizontal line corresponds to $\kappa = 0.38$

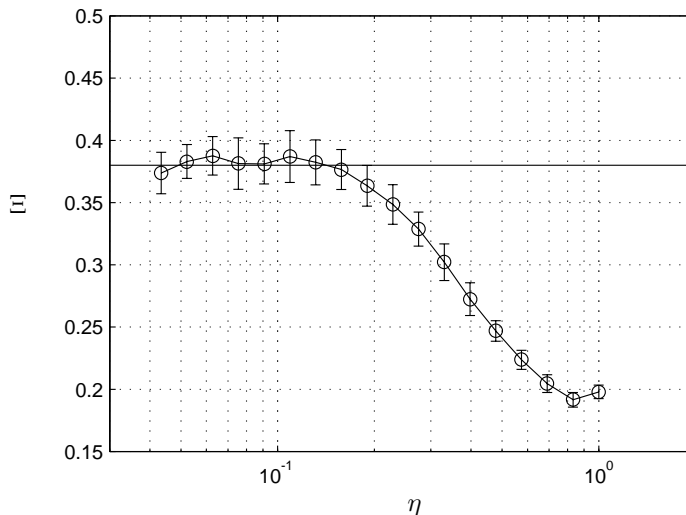


FIGURE 11. Normalized slope of mean profile, Ξ , shown in outer scaling; only the part of the profiles in which $y^+ > 200$ was used and the horizontal line corresponds to $\kappa = 0.38$

Next, the additive constants B and B_1 were investigated by looking at the deviation of the mean velocity profiles, in inner and outer scaling, from the log-profile with the aid of the variables Ψ and Ψ_1 , where

$$\Psi = \overline{U}^+ - \frac{1}{\kappa} \ln y^+ \quad (9)$$

$$\Psi_1 = \frac{U_\infty - \overline{U}}{u_\tau} + \frac{1}{\kappa} \ln \eta \quad (10)$$

The variables Ψ and Ψ_1 are also constant in a region governed by a logarithmic law. The average of the value of Ψ and Ψ_1 , respectively, at a constant wall distance is taken for all Reynolds numbers while omitting the part of the profile where $\eta > M_o$ in the calculation of Ψ and $y^+ < 200$ in the calculation of Ψ_1 . In Figure 12, Ψ is shown with error bars corresponding to the standard deviation. A constant value is found over a wide range in y^+ , again indicating a log-layer. Calculating the average of Ψ within the proposed limits, M_i and M_o , gives $B = 4.1$. In Figure 13 Ψ_1 is presented in the same manner as for Ψ and gives the value of the additive constant in the outer scaled log-law $B_1 = 3.6$. Note that the constant B_1 depends on the definition of δ . Here δ_{95} was used.

In addition to using the above described method to determine the log-law constants, we used the traditional procedure to determine κ and B by performing a least-squares type of fit to the mean velocity profiles. In Figure 14, κ was calculated by fitting a log-law relation for each profile using the following

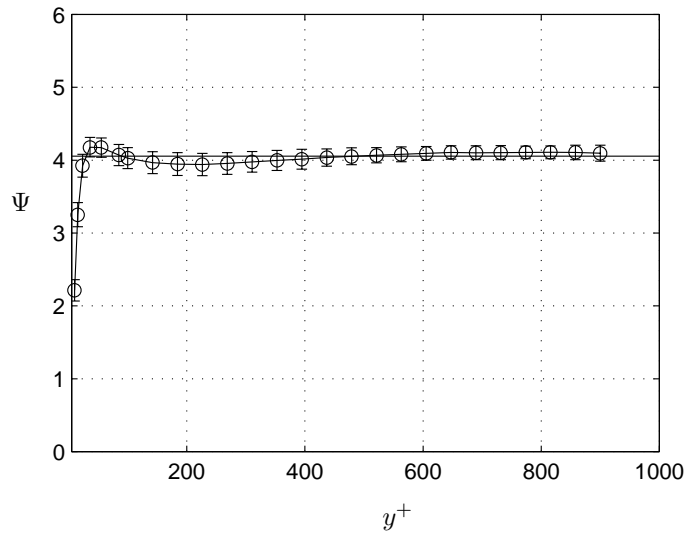


FIGURE 12. The logarithmic intercept Ψ , using $\kappa = 0.38$. The horizontal line corresponds to $B = 4.1$, and the data were evaluated using only the part of the profiles in which $\eta < 0.15$.

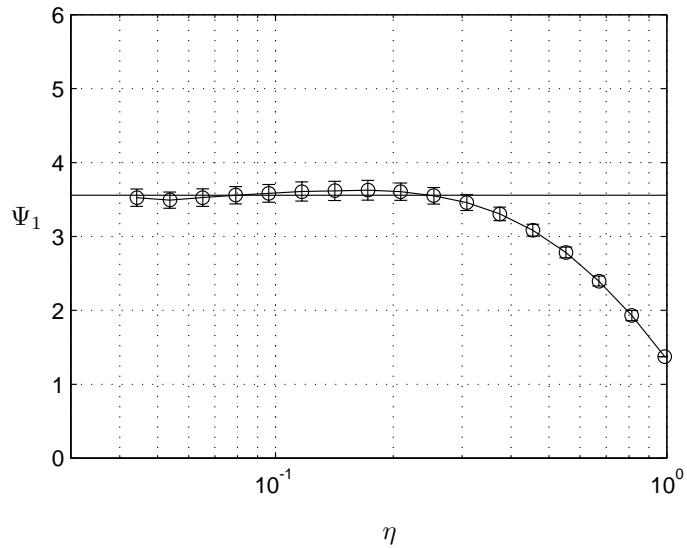


FIGURE 13. The logarithmic intercept Ψ_1 , using $\kappa = 0.38$. The horizontal line corresponds to $B_1 = 3.6$, and the data were evaluated using only the part of the profiles in which $y^+ > 200$.

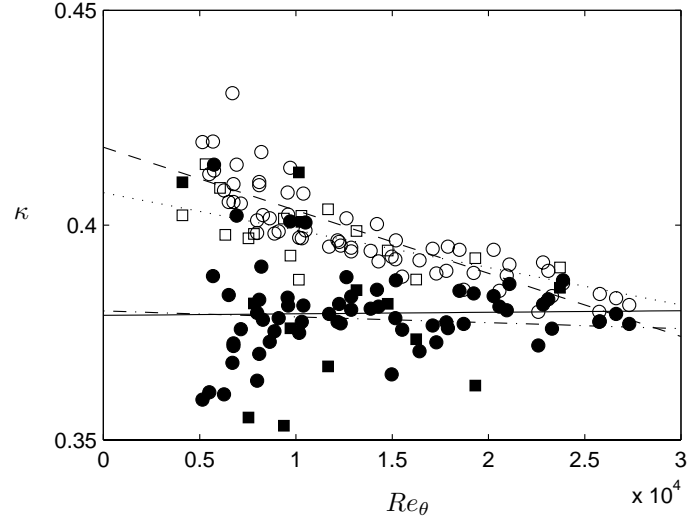


FIGURE 14. The von Kármán constant determined by a least-squares fit, with the outer limit fixed at $\eta = 0.15$ and the inner limit at M_i ; \circ : KTH, $M_i = 50$. \bullet : KTH, $M_i = 200$. Dashed line: KTH, linear fit, $M_i = 50$. Solid line: KTH, linear fit, $M_i = 200$. \square : IIT, $M_i = 50$. \blacksquare : IIT, $M_i = 200$. Dotted line: IIT, linear fit, $M_i = 50$. Dash dotted line: IIT, linear fit, $M_i = 200$.

traditional limits of the fit: $M_i = 50$ and $M_o = 0.15$. The process was also repeated with the newly established limits of $M_i = 200$ and $M_o = 0.15$. The value of κ obtained when using the traditional limits varies with Reynolds number and gives about the commonly used value of 0.41 at low Reynolds numbers. This is then followed by a decreasing trend with increasing Reynolds number. Using the new limits, that are more representative of the logarithmic law, again yields a value of $\kappa \approx 0.38$ independent of Reynolds number.

To investigate the existence of a power-law as proposed recently by several authors Barenblatt (1993); George *et al.* (1997), the following diagnostic function is plotted in Figure 15.

$$\Gamma = \frac{y^+}{U^+} \frac{d\bar{U}^+}{dy^+} \quad (11)$$

The function Γ should be a constant in a region governed by a power-law. However, no region of constant Γ is evident in Figure 6, in particular when compared to Figures 10 and 11. This clearly indicates that a power-law relation is less representative of the entire region of overlap between M_i and M_o .

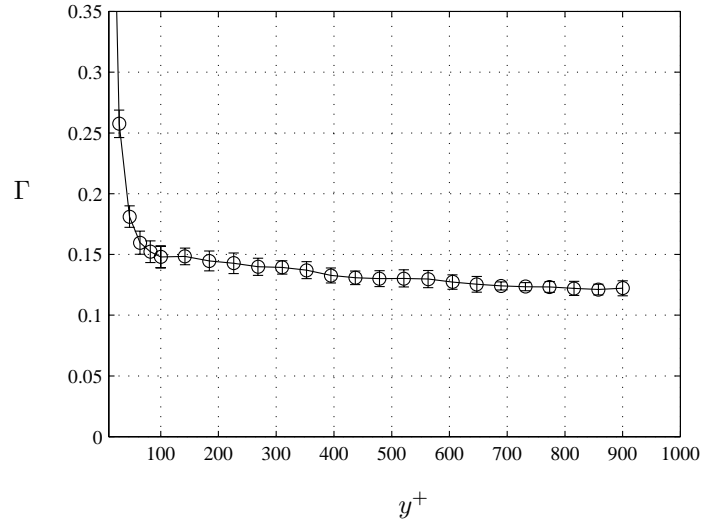


FIGURE 15. The power-law diagnostic function Γ , evaluated using only the part of the profiles in which $\eta < 0.15$.

7. Concluding Remarks

Based on analysis of data from two recent experimental investigations it can be concluded that a logarithmic overlap region, between the inner and outer parts of the mean velocity profiles, exists for $Re_\theta > 6,000$. Establishing, based on the analysis of the data, an inner limit of the region at about $y^+ = 200$ and an outer limit at $\eta = 0.15$ demonstrated the validity of the logarithmic relation. This logarithmic overlap region found differs from that found by Zagarola & Smits (1998a) based on measurements in the Superpipe facility. Where they found the values $\kappa = 0.436$ and $B = 6.15$. This may suggest that the matching of the inner layer with the outer flow results in a slightly different overlap region in the two flow cases; namely, the zero pressure gradient boundary layer and the pressure-gradient driven pipe flow. This is perhaps not totally surprising since the overlap region depends on both the inner and the outer layers and the outer flow is different in the pipe flow from that for the boundary layer. The found value of the von Kármán constant is slightly less than the commonly accepted value of 0.41. Evaluation of the recent high Reynolds number experiment in the German-Dutch wind-tunnel by Fernholz *et al.* (1995) also yields a significantly lower value of the von Kármán constant. Re-evaluation of a carefully selected set of existing experiments would be of great importance for this issue, but out of scope for this article.

8. Acknowledgments

The authors wish to thank Jukka Komminaho and Martin Skote for providing us with DNS data and William Ornt for sharing early versions of his results with us. We wish to thank Mr. Ulf Landen and Mr. Marcus Gällstedt who helped with the manufacturing of the experimental set-up. The support of AFOSR for the IIT experiments is also acknowledged. Financial support from NUTEK and TFR for the KTH experiment is also gratefully acknowledged.

References

- BARENBLATT, G. I. 1993 Scaling laws for fully developed turbulent shear flows. part 1. basic hypotheses and analysis. *J. Fluid Mech.* **248**, 513–520.
- BARENBLATT, G. I. & CHORIN, A. J. 1999 Self-similar intermediate structures in turbulent boundary layers at large reynolds numbers. PAM 755. Center for Pure and Applied Mathematics, University of California at Berkeley.
- COLES, D. E. 1962 The turbulent boundary layer in a compressible fluid. R 403-PR. The RAND Corporation, Santa Monica, CA.
- FERNHOLZ, H. H. & FINLEY, P. J. 1996 The incompressible zero-pressure-gradient turbulent boundary layer: An assessment of the data. *Prog. Aerospace Sci.* **32**, 245–311.
- FERNHOLZ, H. H., JANKE, G., SCHOBBER, M., WAGNER, P. M. & WARNACK, D. 1996 New developments and applications of skin-friction measuring techniques. *Meas. Sci. Technol.* **7**, 1396–1409.
- FERNHOLZ, H. H., KRAUSE, E., NOCKEMANN, M. & SCHOBBER, M. 1995 Comparative measurements in the canonical boundary layer at $re_{\delta_2} < 6 \cdot 10^4$ on the wall of the german-dutch windtunnel. *Phys. Fluids* **7** (6), 1275–1281.
- GEORGE, W. K., CASTILIO, L. & KNECHT, P. 1996 The zero pressure gradient turbulent boundary layer. *Tech. Rep.* TRL-153. Turbulence Research Laboratory, SUNY at Buffalo.
- GEORGE, W. K., CASTILIO, L. & WOSNIK, M. 1997 Zero-pressure-gradient turbulent boundary layer. *Applied Mech. Reviews* **50**, 689–729.
- HITES, M. H. 1997 Scaling of high-reynolds number turbulent boundary layers in the national diagnostic facility. PhD thesis, Illinois Institute of Technology.
- JOHANSSON, A. V. 1992 A low speed wind-tunnel with extreme flow quality - design and tests. In *Prog. ICAS congress 1992*, pp. 1603–1611. ICAS-92-3.8.1.
- KOMMINAHO, J., LUNDBLADH, A. & JOHANSSON, A. V. 1996 Very large structures in plane turbulent couette flow. *J. Fluid Mech.* **320**, 259–285.
- MILLIKAN, C. B. 1938 A critical discussion of turbulent flows in channels and circular tubes. In *Proceedings of the Fifth International Congress of applied Mechanics*.
- NAGIB, H., HITES, M., WON, J. & GRAVANTE, S. 1994 Flow quality documentation of the national diagnostic facility. In *18th AIAA Aerospace Ground Testing Conference, Colorado Springs, CO*. AIAA paper 94-2499.

- ORNT, W. 1999 Measurements of wall-shear stress in turbulent channel and boundary layer flows. Master's thesis, Illinois Institute of Technology.
- ROTTA, J. C. 1950 Über die Theorie der Turbulenten Grenzschichten. Mitt. M.P.I. Ström. Forschung Nr 1, also available as NACA TM 1344.
- SKOTE, M., HENKES, R. & HENNINGSON, D. 1998 Direct numerical simulation of self-similar turbulent boundary layers in adverse pressure gradients. In *Flow, Turbulence and Combustion*, , vol. 60, pp. 47–85. Kluwer Academic Publishers.
- SPALART, P. R. 1988 Direct simulation of a turbulent boundary layer up to $Re_\theta = 1410$. *J. Fluid Mech.* **187**, 61–98.
- ZAGAROLA, M. V. & SMITS, A. J. 1998*a* Mean-flow scaling of turbulent pipe flow. *J. Fluid Mech.* **373**, 33–79.
- ZAGAROLA, M. V. & SMITS, A. J. 1998*b* A new mean velocity scaling for turbulent boundary layers. In *Proceedings of FEDSM'98*.